



## Selection of Conductive Additives in Li-Ion Battery Cathodes

### A Numerical Study

Y.-H. Chen,<sup>a,\*</sup> C.-W. Wang,<sup>a,\*\*</sup> G. Liu,<sup>b</sup> X.-Y. Song,<sup>b</sup> V. S. Battaglia,<sup>b,\*\*</sup> and  
A. M. Sastry<sup>a,c,d,\*\*,z</sup>

<sup>a</sup>Department of Mechanical Engineering, <sup>c</sup>Department of Biomedical Engineering, and <sup>d</sup>Department of Material Science and Engineering, University of Michigan, Ann Arbor, Michigan 48109-2125, USA

<sup>b</sup>Environmental Energy Technologies Division, Lawrence Berkeley National Laboratory, Berkeley, California 94720, USA

The lithium-ion cell has been successively improved with adoption of new cathode electrochemistries, from  $\text{LiCoO}_2$  to higher-capacity  $\text{LiNi}_{1-x}\text{Co}_x\text{O}_2$  to lower cost  $\text{LiNi}_{1-x}\text{Co}_x\text{O}_2$ . The addition of conductive additives to cathode materials has been demonstrated to improve each type. Four systems have emerged as important cathodes in recent studies: (i) the spinel  $\text{LiMn}_2\text{O}_4$ , (ii)  $\text{LiFePO}_4$ , (iii) the “Gen 2” material,  $\text{Li}(\text{Ni}_{0.8}\text{Co}_{0.15}\text{Al}_{0.05})\text{O}_2$ , and (iv) the  $\text{Li}(\text{Ni}_{1/3}\text{Co}_{1/3}\text{Mn}_{1/3})\text{O}_2$  system. The architectures of model composite cathodes were generated using our prior approach in simulating packing of polydisperse arrangements; conductivity was then simulated for several realizations of each case. A key finding was that the conductive coatings significantly improve overall conductivity. Percolation was achieved for the volume fraction of active material ( $\geq 30\%$ ) in studied cases, which was larger than the percolation threshold (29%) for a 3D spherical particulate system. Neither surface nor bulk modifications of active-material particle conductivities seem desirable targets for improvement of laminate conductivity at present. As part of future work, trade-offs between conductivity and capacity will be considered.

© 2007 The Electrochemical Society. [DOI: 10.1149/1.2767839] All rights reserved.

Manuscript submitted March 9, 2007; revised manuscript received May 16, 2007. Available electronically August 24, 2007.

The lithium-ion cell has been successively improved incrementally with adoption of new cathode electrochemistries, from  $\text{LiCoO}_2$ <sup>1</sup> to higher-capacity  $\text{LiNi}_{1-x}\text{Co}_x\text{O}_2$ <sup>2-4</sup> to lower cost  $\text{LiNi}_{1-x}\text{Co}_x\text{O}_2$ .<sup>5,6</sup> However, capacity fade and/or uncontrolled generation of flammable gases during operation remain persistent problems. The addition of conductive additives to cathode materials has been demonstrated to improve capacity, via reduction of internal resistance, and cyclability.

Typical materials (Table I)<sup>7-14</sup> include carbon black (as an additive or a coating on cathode particles or current collectors) and graphite nonaqueous ultrafine carbon (UFC) suspensions. Selection of optimal combinations of conductive additives, though, remains challenging, as choices of materials and architectures have grown dramatically.

Gains have been achieved using multiple schema for loading with conductive additives, as summarized by Fig. 1.<sup>15</sup> Performance has been improved by several measures in different systems. But the relative gains in addition of additives, including methods by which they can be added, have not been studied, though measurement of conduction has improved.<sup>16</sup>

Four systems have emerged as important cathodes in recent studies (Table II): (i) the spinel  $\text{LiMn}_2\text{O}_4$ ,<sup>17,18</sup> (ii)  $\text{LiFePO}_4$ ,<sup>19,20</sup> (iii) the “Gen 2” material,  $\text{Li}(\text{Ni}_{0.8}\text{Co}_{0.15}\text{Al}_{0.05})\text{O}_2$ , put forward by the Department of Energy’s Advanced Technology Development program based at Argonne National Laboratories,<sup>21,22</sup> and (iv) the “1/3, 1/3, 1/3” system,  $\text{Li}(\text{Ni}_{1/3}\text{Co}_{1/3}\text{Mn}_{1/3})\text{O}_2$ .<sup>23,24</sup> The strengths of these systems include, respectively, lost cost, high rate ( $\text{LiMn}_2\text{O}_4$ <sup>17,18</sup>); low cost, high energy density ( $\text{LiFePO}_4$ ,<sup>19,20,25</sup>), high energy, high power [ $\text{Li}(\text{Ni}_{0.8}\text{Co}_{0.15}\text{Al}_{0.05})\text{O}_2$ ,<sup>21,22</sup>]; and high energy, high capacity, and good cycle performance [ $\text{Li}(\text{Ni}_{1/3}\text{Co}_{1/3}\text{Mn}_{1/3})\text{O}_2$ ,<sup>23,24</sup>].

Achievement of sufficient conductivity first requires attainment of percolation in a conductive phase,<sup>26-28</sup> a problem studied extensively for anode materials and generically for a variety of shapes of particles.<sup>29-32</sup> There have also been published studies of specific cathode materials and loading schema.<sup>12,33</sup> Both particle shape and loading type are required in order to identify percolation onset and optimize addition of conductive particles by type and method beyond the percolation point. Even percolation onset is strongly af-

ected by relatively minor changes in particles shape; for example, the percolation threshold is reduced from 30 to 10% as particle aspect ratio ( $a/c$ ,  $a$  is the major axis length and  $c$  is the minor axis length of the ellipsoid). Domain length to particle diameter ( $L/D$ ) increases from 1 to 6.<sup>29</sup> It can thus be presumed that alterations in loading method have a similarly strong effect on percolation onset

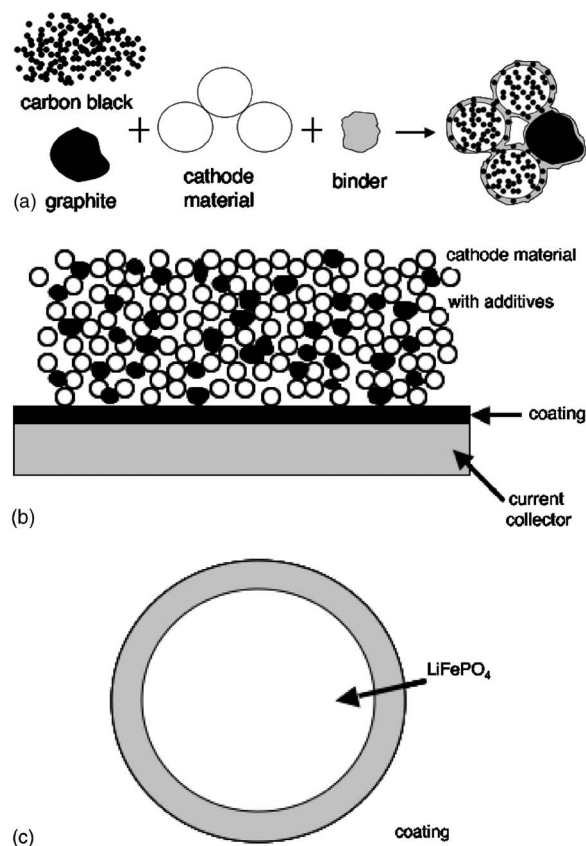


**Figure 1.** Possible ways of incorporating conductive additives: (a) addition of large (graphite) and small particles (carbon blacks), (b) current collector coating, and (c) coating of the cathode particles.<sup>15</sup>

\* Electrochemical Society Student Member.

\*\* Electrochemical Society Active Member.

<sup>z</sup> E-mail: amsastry@umich.edu

**Table I. Improved performance by adding different additives in different cathode materials.**

Cathode material	Theoretical capacity (mAh/g)	Ref.	Additive	Amount (wt %)	Performance enhancement		
					Capacity (mAh/g)	Conductivity	Others
LiCoO <sub>2</sub>	274	7	Carbon	5–10	158	-	-
		8	Carbon black	5	-	-	Slight improvement in cyclability from 125 to 133 mAh/g in 10 cycles
LiMn <sub>2</sub> O <sub>4</sub>	148	7	Carbon black	10	129	-	Improvement in cyclability from 90 to 110 mAh/g in 50 cycles
		9	Carbon black	32.2	135	-	-
		10	Nonaqueous ultrafine carbon with TAB2	20 (1:3–1:1)	130	-	-
		11	Carbon black	10	130	-	-
		12	Carbon black	25 (v.f.)	120	Conductivity increase: 10 <sup>-5</sup> to 1 S/cm	-
		8	Carbon black	10	-	Conductivity increase: 2.5 × 10 <sup>-3</sup> to 0.4 S/cm	-
LiFePO <sub>4</sub>	170	13	Carbon black	31	-	Conductivity increase: 5 × 10 <sup>-8</sup> to 0.1 S/cm	-
		14	Carbon black graphite	6 6	160	Resistance decrease: 140 to 80 W cm <sup>2</sup>	-

and overall conductivity. However, the conductance of gap regions, as opposed to simple bulk conduction, must also be modeled and mapped to experimental findings. Additionally, methods are needed to incorporate the polydisperse, multiphase materials already in use, in order to reduce costly experimentation.

Our present study was focused on the four electrochemistries mentioned earlier: LiFePO<sub>4</sub> (Hydro-Quebec, Inc., Quebec, Canada), LiMn<sub>2</sub>O<sub>4</sub> (Toda Co. Ltd., Japan), Li(Ni<sub>0.33</sub>Co<sub>0.33</sub>Mn<sub>0.33</sub>)O<sub>2</sub> (Seimi Chemical Co. Ltd, Kanagawa, Japan), and Li(Ni<sub>0.8</sub>Co<sub>0.15</sub>Al<sub>0.05</sub>)O<sub>2</sub> (Fuji Chemical Industry Co., Ltd.). The carbon black (Shawinigan) or graphite (SFG-6) was used as conductive additive. Poly(vinylidene fluoride) (PVDF, Kureha) was used as binder. Particle sizes and mass densities for each material are listed in Table III.<sup>34-36</sup> We had two main objectives with the present work: (i) to predict the conductivity of cathodes with different amounts, types, and architectures of conductive additives and active materials and (ii) to iden-

tify the best blends of active materials, conductive additives, and binder to achieve the highest conductivity among combinations studied.

## Methods

Conduction experiments in our prior work<sup>31</sup> and others<sup>36</sup> have established baseline conductivities of materials. For packed particle arrangements, our prior model for packing<sup>32</sup> was used to construct the polydisperse structures of the model cathode systems, following classic and more recent work on numerical simulation of complex structures.<sup>32,37-41</sup> A voxelated finite element method was used to determine the effective conductivity of the multiphases networks in order to meet our second objective of determining best blends of conductive additives among those studied.

**Table II. Important cathodes in recent studies.**

Cathode material	Ref.	General properties	Producer	Targeted applications
LiMn <sub>2</sub> O <sub>4</sub>	17 and 18	Low capacity, high rate, low cost	Toda	High power
LiFePO <sub>4</sub>	19, 20, and 25	High energy density, low electronic conductivity, low cost	Hydro-Quebec	High energy or high power
Li(Ni <sub>0.8</sub> Co <sub>0.15</sub> Al <sub>0.05</sub> )O <sub>2</sub>	21 and 22	High specific energy, high power	Fuji	High energy or high power
Li(Ni <sub>1/3</sub> Co <sub>1/3</sub> Mn <sub>1/3</sub> )O <sub>2</sub>	23 and 24	High energy, high capacity, good cycle performance	Seimi	High energy

**Table III. Particle size (μm), mass density (g/cm<sup>3</sup>), and bulk conductivities (S/m) of different active materials and graphite.**

Material	LiMn <sub>2</sub> O <sub>2</sub>	LiFePO <sub>4</sub>	Li(Ni <sub>0.8</sub> Co <sub>0.15</sub> Al <sub>0.05</sub> )O <sub>2</sub>	Li(Ni <sub>1/3</sub> Co <sub>1/3</sub> Mn <sub>1/3</sub> )O <sub>2</sub>	Graphite <sup>34</sup>
Particle size (μm)	8.96	6.41	10.17	11.04	7.45
Mass density (g/cm <sup>3</sup> )	4.28	3.58	2.28	4.75	1.95
Bulk conductivity (S/m)	5.56 × 10 <sup>-4</sup>	5.91 × 10 <sup>-1</sup>	4.00 × 10 <sup>-2</sup>	1.06 × 10 <sup>-3</sup>	-
Conductivity from ref. (S/m)	10 <sup>-4</sup> –10 <sup>-335</sup>	10 <sup>-936</sup>	-	-	1.67 × 10 <sup>4</sup>

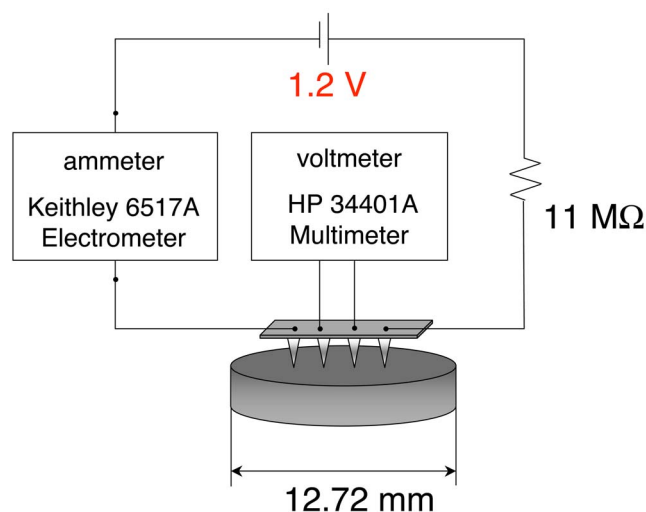


**Figure 2.** (Color online) Schematic illustration of the configuration in conductivity measurement.

*Experimental.— Measurement of conductivity.*— Electronic properties of cathode materials have not been widely reported. Importantly, it has been established in the presently studied cathode materials that manufacturing methods affect conductive properties.<sup>42,43</sup> The materials studied were prepared and tested for their conductive properties. This approach was designed to reduce variability and allow application of classic theory in conduction to determine conductivity of the bulk phase.

Powders of active materials were placed into a round die of inner diameter 12.72 mm and compressed with a force of 9.8–29.4 kN at 25°C for 5 min to achieve various densities using Carver Laboratory Press model 2699. Pellet densification reduces particle separation distance and gap resistance<sup>44</sup> and generally is used to improve the accuracy of measured bulk conductivity.

The conductivity of a pellet was measured using an inline four-point-probe technique.<sup>31</sup> A schematic of the experiment is shown in Fig. 2. A current was delivered and withdrawn from the outer two probes; the voltage difference was measured from the inner two probes. The current source was a 1.2 V AAA NiMH battery (Radio Shack) in series with resistance of 11 MΩ. A Keithley 6517 A electrometer and an HP 34401 A multimeter were used to measure the current and the voltage, respectively. The conductivity of the pellet was calculated<sup>45</sup> via

$$\sigma_e = \frac{I}{4.532tV} \quad [1]$$

where  $\sigma_e$  is the conductivity of the pellet in S/mm,  $t$  is the thickness of the pellet in mm,  $I$  is the current measured in amps, and  $V$  is the voltage measured in V. Equation 1 is valid for a single-layer specimen.

For porous materials, Bruggeman<sup>46</sup> classically found that the effective conductivity,  $\sigma_e$ , is related to the bulk conductivity,  $\sigma_0$ , and the volume fraction of the solid phase,  $\varepsilon$ , as

$$\sigma_e = \sigma_0 \varepsilon^\alpha \quad \text{where } \alpha = 1.5 \quad [2]$$

where  $\alpha$  is the Bruggeman exponent, a curve-fitting parameter for experimental results. Volume fraction  $\varepsilon$  is calculated from

$$\varepsilon = \frac{D_p}{D_B} \quad [3]$$

where  $D_p$  and  $D_B$  are the density of pellet and density of bulk material, respectively, whereupon bulk conductivity is determined directly.

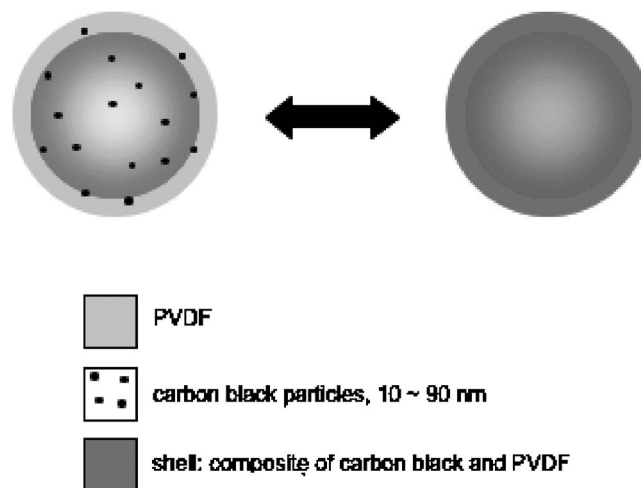


**Figure 3.** Schematic diagram of coating of carbon black/PVDF.

*Measurement of particle shape and size.*— Particle size distributions (PSD) were quantified using a Beckman Coulter LS230 laser diffraction particle size analyzer, with a measurement range between ~0.04 and 2000 μm. Sample powders of 0.05–0.10 g were mixed with 100 mL distilled water beaker where 5 drops Darvan C were used as a dispersant; uniformity was achieved with approximately 15 min of ultrasonic mixing.

*Simulations.— Packing algorithm.*— The architecture of the composite cathode, comprised of active material, graphite, carbon black, and PVDF, was generated using our prior approach.<sup>32</sup> The general procedure is summarized briefly as follows. Sizes and numbers of particles in each phase, as determined by the PSD and designated volume fraction, were initially placed randomly in a representative volume. Particles were simulated as spheres, ellipsoids, or coated objects. Repulsive forces between particles were applied to correct initial overlaps.

During the Li-ion cell preparation, all constituents were fully mixed, leaving, presumably, active material particles coated with composites of PVDF and carbon black. Carbon black particles are typically 10–90 nm<sup>47</sup> in diameter; the typical aggregate size of carbon black is 100–300 nm,<sup>47</sup> though the primary aggregate may fracture during mixing.<sup>47</sup> Thus, a mixture of carbon black and polymer binder was approximated as a coating surrounded other particles, as shown in Fig. 3. This also allowed creation of simulations that were identical to experimental volume fractions.

Periodic boundary conditions and the collision algorithm were applied to achieve computational efficiency and fidelity to experimental conditions. The representative volume in this study was set to  $1 \times 1 \times 2$  unit<sup>3</sup>. Periodic boundary conditions were assigned in the  $x$  and  $y$  directions to reduce the size of the simulation domain. The length of the representative volume in the  $z$  direction was set at a minimum of twice the length of each of the other two directions because of the lack of a periodic boundary in that direction. The collision process was terminated when the total volume fraction of the unit volume in the middle portion of the representative volume in the  $z$  direction was equal to the assigned volume fraction.

Relative sizes of materials are illustrated in Table III. The radius of active materials was set to 0.15 of the representative volume; the semi-axes of graphite were dependent upon the size of active materials. The graphite was represented as a disklike ellipsoid with aspect ratios  $a/b$ ,  $a/c$ , and  $b/c$  ( $a$ ,  $b$ , and  $c$  are the length of three semi-axes) set to 1, 7.4, and 7.4, respectively. The mixture of the carbon black and PVDF was simulated as a coating around the active material and graphite particles. Table IV lists factors (volume fraction of active material, porosity, graphite, and ratio of PVDF and carbon black) and levels of each. The volume fraction of carbon

Table IV. List of simulation cases for each active material.

Factor	Level
Porosity (v.f. %)	40
	50
Active material (v.f. %)	30
	40
	50
Graphite (v.f. %)	0
	2.5
	5
	7.5
PVDF/C	1.22
	2.74
	5.48

black and PVDF could be determined if porosity, the amount of active material, and the ratio of carbon black and PVDF were determined. Three simulation realizations were generated for each permutation of conditions studied.

**Conductivity modeling.**—The active material and conductive additives particle aggregates are separated by an interfacial polymer layer. This feature is generally attributed to the occurrence of a tunneling effect through the insulating polymer. Combined with the conduction percolation through the aggregates, this phenomenon is known as “tunneling percolation.”<sup>47</sup> The tunneling effect between paired particles can be simulated with assignment of a gap resistance. The value of this gap resistance depends on contact pressure, distance, and material properties of the contacting particles and polymer interface.<sup>44</sup> In the cases studied here, the gap resistance was assumed to be zero, since cathodes were usually prepared with application of high compression pressure to reduce the distance among the packed particles, and the mixture of carbon black and PVDF served as coating around the particles binding particles directly. The current between contact surfaces is defined by

$$(V_a - V_b) = iR \quad [4]$$

where  $i$  is the current in amps,  $V_a$  and  $V_b$  are the electrical potentials on the points of both side of the contact surfaces in V, and  $R$  is the gap resistance in  $\Omega$ .

Bulk conductivities of different active materials measured from experiments were assigned to corresponding phases. Figure 4 shows the conductivities of mixtures of carbon black and PVDF. In simulations, the conductivities of PVDF and carbon black were assigned three levels, as shown in Table IV, depending upon the ratio of PVDF and carbon black.

**Model generation and analysis.**—Finite element meshing was performed using a voxelation method to prevent mesh-induced singularities. The representative volume was set to  $1 \times 1 \times 2$  unit<sup>3</sup>. Voxels of  $100 \times 100 \times 100$  were assigned to a unit volume, which was the middle portion of the representative volume in the  $z$  direction. Assuming the representative volume in the  $z$  direction ranged from 0 to 2 units, the middle section was between 0.5 and 1.5 units in the  $z$  direction. A cubic element of length of 0.01 units enclosing the voxel was generated with an assigned electronic conductivity.

Because the form of the governing equations for heat transfer and electronic conductivity are identical, the existing heat-transfer analysis in the finite element package ABAQUS/STANDARD was used<sup>48</sup> for steady-state analysis, with heat flux and current flux governing equations

$$J = -\sigma_1 \nabla V \quad [5]$$

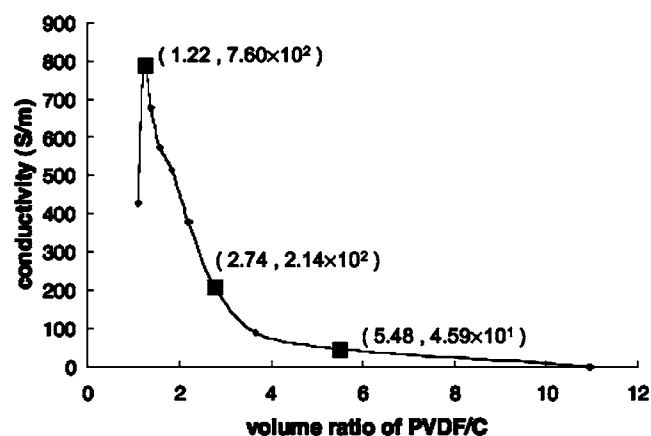


Figure 4. Conductivities of different combinations of carbon black and PVDF.

$$F = -\sigma_2 \nabla T \quad [6]$$

where  $\sigma_1$  is the electronic conductivity in S/m,  $J$  is the current density in A/m<sup>2</sup>,  $V$  is the electrical potential drop in V along its length,  $\sigma_2$  is the thermal conductivity in W/m K,  $F$  is the heat flux in W/m<sup>2</sup>, and  $T$  is the temperature drop in K. Wall boundary conditions were set as 0 and 1 K, respectively, at  $x = 0$  and 1. The total heat flux in the  $x$  direction was calculated, whereupon effective conductivity of the cubic unit volume was determined via Eq. 6.

## Results

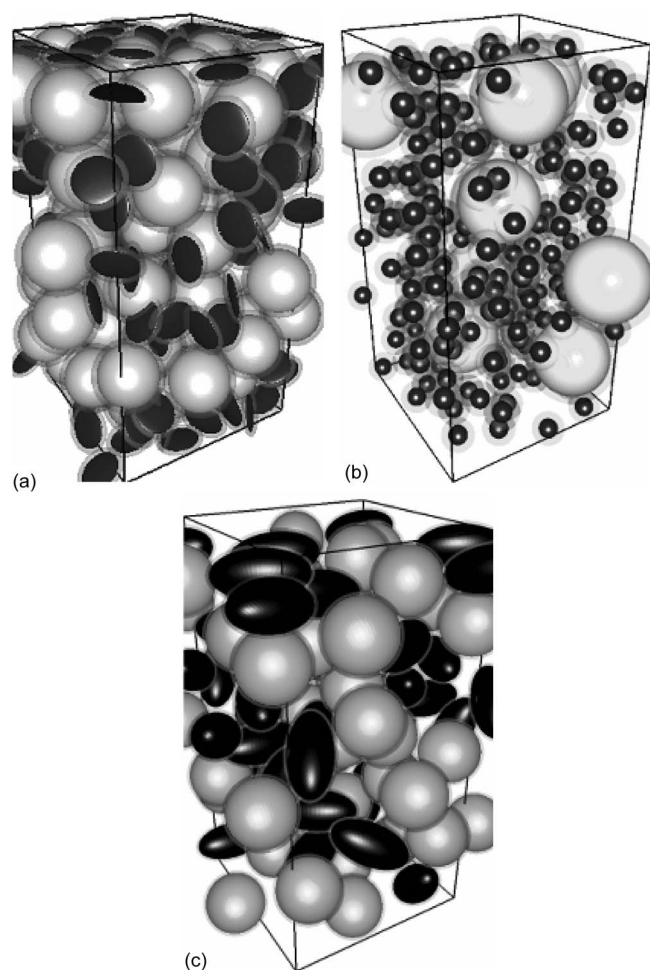
Table III contains material properties, particle sizes, densities, and bulk conductivities used in simulations. Figure 4 reports the bulk conductivity of the carbon black and PVDF mixture. Increasing the carbon black content by 30 volume fraction (v.f) % resulted in a 16-fold increase in conductivity. The only exception to this trend was for a 1:1 ratio of PVDF to carbon, where measured conductivity dropped to 420 S/m, i.e., the same value as for the 2.2:1 ratio.

Figure 5 shows examples of various microstructures (comprised of spherical active materials, graphite particles, and coated mixture of carbon black and PVDF) generated from collision modeling. Figure 5a illustrates an example of the microstructure of percolated network studied in the present work. Figures 5b and c illustrate the significant microstructural differences in materials of identical volume fraction but different particle shapes and sizes.

The voxelated finite element model of Fig. 6a and b is an example of a multiphase analysis used to avoid mesh singularities around the contact region. Figure 6a shows the temperature distribution of core material for a structure comprised of 30% active material, 7.5% graphite, and 40% porosity. Figure 6b shows the temperature distribution of coatings for a volume composition of 10.15% carbon black and 12.35% PVDF.

Simulation results of normalized conductivities of LiMn<sub>2</sub>O<sub>4</sub> system for various combinations of active materials, graphite, carbon black, and PVDF are reported in Fig. 7. Averaged data were plotted in the figures, with error bars of  $\pm 1 \sigma$  (standard deviation). Figures of results of other systems are omitted for brevity, because trends were similar; numerical results are reported in Tables V-VIII.

Averaged normalized simulation results of conductivity with 40 and 50% porosity are presented in Tables V-VIII. These tables report averaged, normalized conductivities for specific combinations of active material, graphite, and ratios of PVDF to carbon black. The two-way statistical analyses (by SPSS 12.0<sup>49</sup>) of the simulation data are also given in Tables V-VIII. The statistical analyses in term of  $p$  values allow determination of the significance of the effects of additives. Factors are considered significant if  $p$  is smaller than 0.05. The  $p$  values in rows denote the effect of increase in the ratio of



**Figure 5.** Packing simulations with different constituents: (a) 60 v.f.% mixture of spheres and platelets, representing cathode active material and graphite, (b) 40 v.f.% mixture of two different sizes, representing cathode active materials and carbon black, and (c) 40 v.f.% mixture of ellipsoids and spheres, representing spherical cathode active materials and ellipsoidal graphite fiber.

PVDF to carbon black on normalized conductivity. The  $p$  values in columns denote the effect of increase in the volume fraction of graphite on normalized conductivity.

The statistical analysis results in Tables V-VIII show that volume fraction of graphite is significant for conductivity in some cases with 30% active material. For example, in Table VII, with 40% porosity, 30% active material, and PVDF/C of 1.21, the  $p$  value of 0.001 denotes the significant effect of increase in the volume fraction of graphite on the normalized conductivity. For this composition, the normalized conductivity increases from  $4.03 \times 10^{-3}$  to  $1.21 \times 10^{-2}$  with an increase in graphite from 0 to 7.5%.

The statistical analysis results in Tables V-VIII show that the ratio of PVDF to carbon black is the most significant factor affecting conductivity. Values of  $p < 0.05$  can be seen in almost every row in Tables V-VIII. For example, in Table VI, with 40% porosity, 30% active material, and 2.5% graphite, the  $p$  value of 0.005 indicates the significant effect of increase in the volume ratio of PVDF to carbon black on the normalized conductivity. In this composition, the normalized conductivity increases from  $1.74 \times 10^{-4}$  to  $2.28 \times 10^{-3}$  with a reduction in volume ratio from 5.48 to 1.21.

Indeed, addition of graphite actually reduces conductivity when the PVDF coating is penalized for the addition of graphite. For example, in Table VII, with 40% porosity, 50% active material, and PVDF/C of 1.21, a  $p < 10^{-4}$  denotes the significant effect of in-

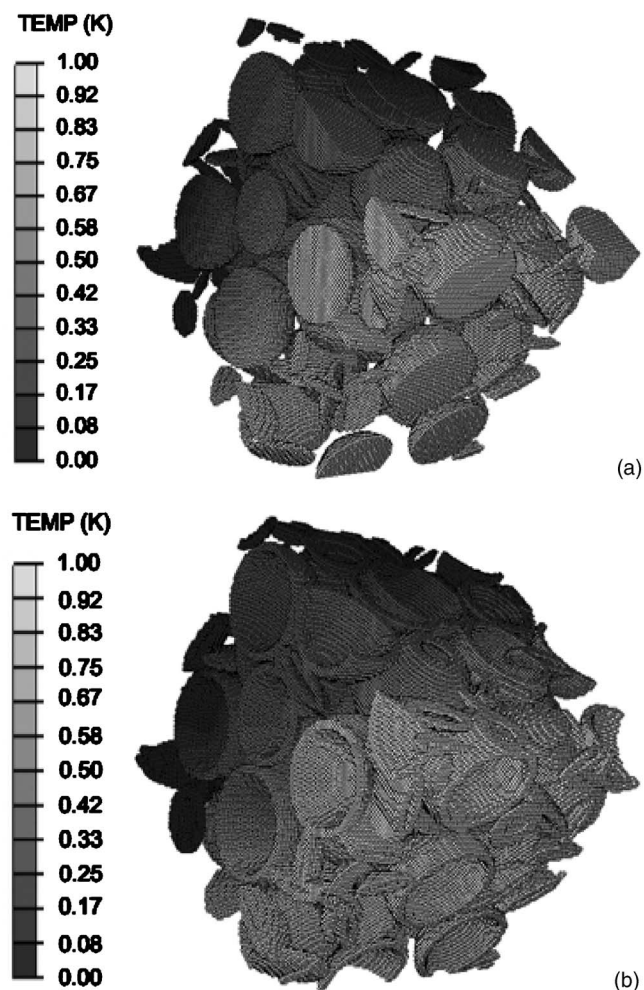


**Figure 6.** Temperature distribution from finite element analyses, structure of 40% porosity; 30 v.f.% active material, 7.5 v.f.% graphite, 10.15 v.f.% carbon black, and 12.35 v.f.% PVDF showing in (a) core material (active material and graphite) and (b) coatings (carbon black and PVDF).

crease in the volume fraction of graphite on the normalized conductivity. In this composition, the normalized conductivity decreases from  $1.24 \times 10^{-3}$  to  $1.18 \times 10^{-4}$  with increase in graphite from 0 to 5%; meanwhile, because of increase in graphite, carbon black decreases from 4.51 to 2.26% and PVDF decreases from 5.49 to 2.74%. The effect of reduction of conductivity can be found in cases with 40% porosity and 50% active material shown in Table V, VI, and VII.

### Discussion

Simulations of the computational intensity described here must necessarily represent rather small volumes; thus, examination of size effect is critical. Prior studies of overlapping<sup>29</sup> and nonoverlapping<sup>50</sup> spherical particles have shown that the error due to size effect of the domain is negligible for the ratio  $L/d$  (domain length to particle diameter)  $> 2.5$ . The error in determination of effective properties was specifically found to be  $< 1.8\%$  for a periodic elastic composite with a disordered unit cell of a random dispersion of nonoverlapping identical spheres,<sup>50</sup> a similar system to simulations presented here. In all simulations here, the ratio of  $L/d > 3.3$  was used to prevent any introduction of error.

Differences in arrangements of statistically similar structures, along with contrast ratios of properties in phases, result in variances in predicted effective properties in heterogeneous materials. These increased variances can be explained in terms of percolation of

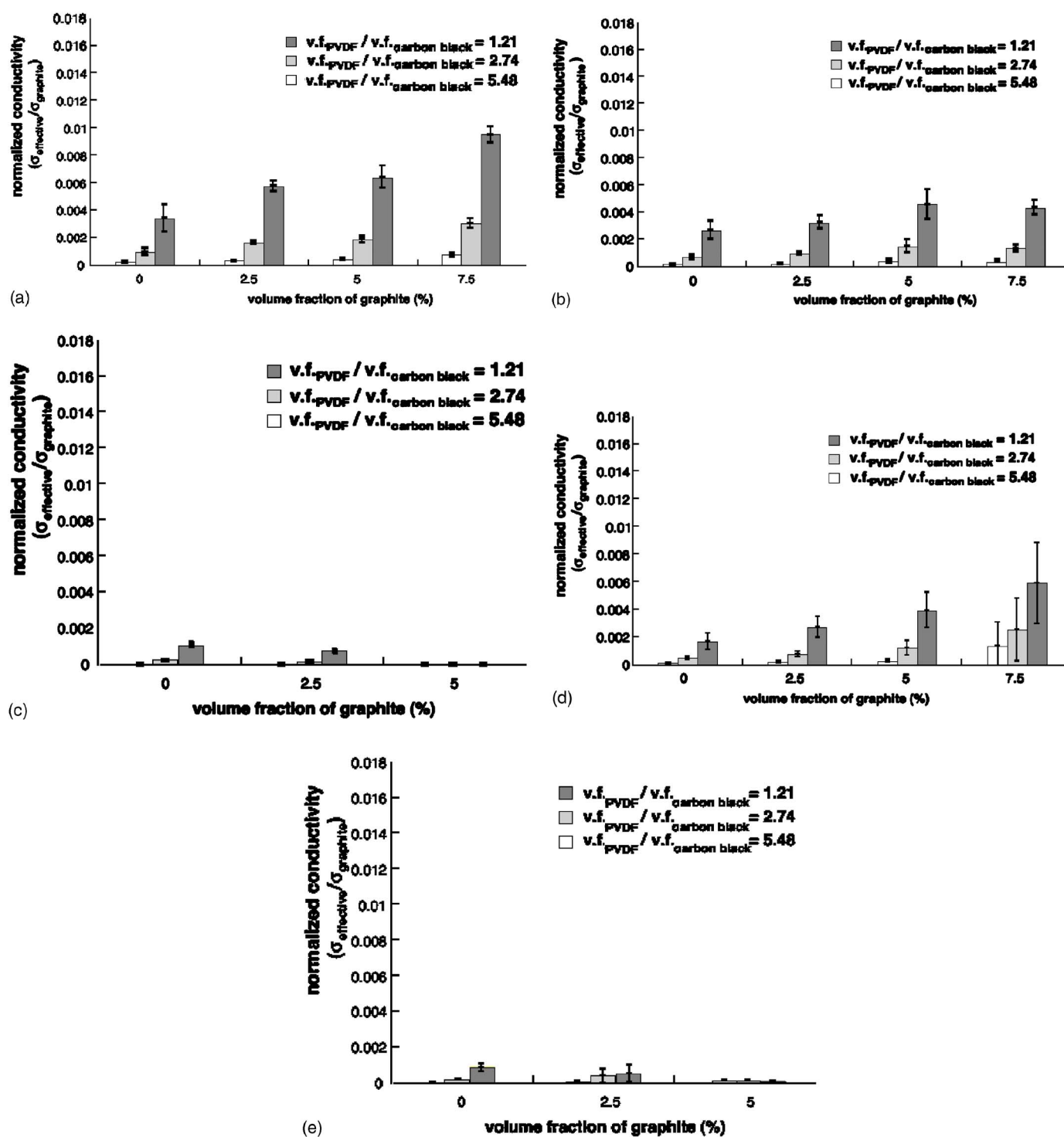


**Figure 7.** Conductivity of composite LiMn<sub>2</sub>O<sub>4</sub> with (a) 40% porosity and 30% active material, (b) 40% porosity and 40%, active material, (c) 40% porosity and 50% active material, (d) 50% porosity and 30% active material, and (e) 50% porosity and 40% active material.

phases in each case. Because achievement of percolation is probabilistic in finite volumes, resulting conductivity is typically highly variable close to the percolation point. Here, results showed highest variability at the closest value to the percolation point studied for graphite (7.5% for the present study as compared to 10% being the theoretical percolation point for particles with an aspect ratio of 7.4<sup>29</sup>).

Increasing the volume fraction of carbon black and PVDF appears to be the best strategy in improving overall conductivity for

the materials and ranges of volume fractions studied. Active material particles, made conductive with a coating of carbon black and PVDF, achieved percolation because the volume fraction in studied cases ( $\geq 30\%$ ) was larger than the percolation threshold (29%) for a 3D spherical particulate system.<sup>29</sup> This loading scheme can be thought of as achieving percolation in a system of hollow, conductive spheres, with the path of least resistance of electrons through the coating.

**Table V. Simulation results and two-way statistical analyses of the simulation data in terms of  $p$  values of normalized conductivity of composite  $\text{LiMn}_2\text{O}_2$  with 40% porosity and 50% porosity.**

Porosity	$\text{LiMn}_2\text{O}_4$	PVDF/C	Graphite (%)				$p$
			0	2.5	5	7.5	
40%	30%	1.21	$4.5 \times 10^{-3}$	$5.75 \times 10^{-3}$	$6.77 \times 10^{-3}$	$9.60 \times 10^{-3}$	$<10^{-4}$
		2.74	$1.21 \times 10^{-3}$	$1.62 \times 10^{-3}$	$1.96 \times 10^{-3}$	$2.93 \times 10^{-3}$	$<10^{-4}$
		5.48	$2.59 \times 10^{-4}$	$3.52 \times 10^{-4}$	$4.30 \times 10^{-4}$	$6.65 \times 10^{-4}$	$<10^{-4}$
		$p$	0.002	$<10^{-4}$	$<10^{-4}$	$<10^{-4}$	
	40%	1.21	$1.94 \times 10^{-3}$	$2.75 \times 10^{-3}$	$3.40 \times 10^{-3}$	$3.79 \times 10^{-3}$	0.04
		2.74	$5.23 \times 10^{-4}$	$7.64 \times 10^{-4}$	$9.92 \times 10^{-4}$	$1.08 \times 10^{-3}$	0.05
		5.48	$1.12 \times 10^{-4}$	$1.67 \times 10^{-4}$	$2.20 \times 10^{-4}$	$2.36 \times 10^{-4}$	0.01
		$p$	0.001	$<10^{-4}$	0.001	$<10^{-4}$	
	50%	1.21	$1.28 \times 10^{-3}$	$8.82 \times 10^{-4}$	$1.82 \times 10^{-5}$	-	$<10^{-4}$
		2.74	$3.46 \times 10^{-4}$	$2.40 \times 10^{-4}$	$5.06 \times 10^{-6}$	-	$<10^{-4}$
		5.48	$7.38 \times 10^{-5}$	$5.13 \times 10^{-5}$	$1.21 \times 10^{-6}$	-	$<10^{-4}$
		$p$	$<10^{-4}$	$<10^{-4}$	0.03	-	
50%	30%	1.21	$1.57 \times 10^{-3}$	$2.94 \times 10^{-3}$	$5.16 \times 10^{-3}$	$9.24 \times 10^{-3}$	0.06
		2.74	$4.23 \times 10^{-4}$	$8.18 \times 10^{-4}$	$1.75 \times 10^{-3}$	$5.12 \times 10^{-3}$	0.2
		5.48	$9.04 \times 10^{-5}$	$1.77 \times 10^{-4}$	$4.42 \times 10^{-4}$	$3.55 \times 10^{-3}$	0.4
		$p$	0.003	0.001	0.003	0.1	
	40%	1.21	$1.12 \times 10^{-3}$	$8.56 \times 10^{-4}$	$2.28 \times 10^{-4}$	-	0.05
		2.74	$3.02 \times 10^{-4}$	$2.34 \times 10^{-4}$	$6.33 \times 10^{-5}$	-	0.2
		5.48	$6.46 \times 10^{-5}$	$5.02 \times 10^{-5}$	$1.37 \times 10^{-5}$	-	0.2
		$p$	$<10^{-4}$	0.4	0.3	-	

Clearly, there is an important tradeoff in considering the type of additive to use. It is advantageous to use highly conductive surface coatings, vs using larger particle conductive additives dispersed among active material particles, in many ranges studied. As demonstrated by calculated  $p$  values in Tables V-VIII, increasing the thickness of coatings improves conductivity for all cases studied, with the

exception of cases with 40% porosity, 50% active material, and 5% graphite, as shown in Table V, VII, and VIII. In these cases, the coating thickness amounted to only 0.082, 0.091, and 0.097  $\mu\text{m}$ , respectively, or 0.92, 0.89, and 0.87%, respectively, of the diameter of a typical active-material particle. It seems likely that imperfections in coatings for these thin layers would substantially reduce the

**Table VI. Simulation results and two-way statistical analyses of the simulation data in terms of  $p$  values of normalized conductivity of composite  $\text{LiFePO}_4$  with 40% porosity and 50% porosity.**

Porosity	$\text{LiFePO}_4$	PVDF/C	Graphite (%)				$p$
			0	2.5	5	7.5	
40%	30%	1.21	$2.22 \times 10^{-3}$	$2.88 \times 10^{-3}$	$7.84 \times 10^{-3}$	$1.47 \times 10^{-2}$	0.05
		2.74	$6.01 \times 10^{-4}$	$7.97 \times 10^{-4}$	$2.40 \times 10^{-3}$	$5.80 \times 10^{-3}$	0.05
		5.48	$1.30 \times 10^{-4}$	$1.74 \times 10^{-4}$	$5.53 \times 10^{-4}$	$1.89 \times 10^{-3}$	0.02
		$p$	0.02	0.005	$<10^{-4}$	0.03	
	40%	1.21	$2.45 \times 10^{-3}$	$3.41 \times 10^{-3}$	$4.70 \times 10^{-3}$	$6.49 \times 10^{-3}$	0.005
		2.74	$6.64 \times 10^{-4}$	$9.50 \times 10^{-4}$	$1.38 \times 10^{-3}$	$2.26 \times 10^{-3}$	0.06
		5.48	$1.46 \times 10^{-4}$	$2.13 \times 10^{-4}$	$3.23 \times 10^{-4}$	$6.17 \times 10^{-4}$	0.3
		$p$	$<10^{-4}$	$<10^{-4}$	$<10^{-4}$	0.07	
	50%	1.21	$8.92 \times 10^{-4}$	$7.19 \times 10^{-4}$	$6.68 \times 10^{-5}$	-	0.002
		2.74	$2.45 \times 10^{-4}$	$2.09 \times 10^{-4}$	$5.86 \times 10^{-5}$	-	0.004
		5.48	$5.68 \times 10^{-5}$	$5.64 \times 10^{-5}$	$3.35 \times 10^{-5}$	-	0.03
		$p$	0.002	$<10^{-4}$	$<10^{-4}$	-	
50%	30%	1.21	$2.54 \times 10^{-3}$	$2.25 \times 10^{-3}$	$3.70 \times 10^{-3}$	$6.64 \times 10^{-3}$	0.2
		2.74	$6.87 \times 10^{-4}$	$6.20 \times 10^{-4}$	$1.06 \times 10^{-3}$	$3.05 \times 10^{-3}$	0.3
		5.48	$1.50 \times 10^{-4}$	$1.37 \times 10^{-4}$	$2.41 \times 10^{-4}$	$1.05 \times 10^{-3}$	0.3
		$p$	0.02	0.001	0.003	0.04	
	40%	1.21	$9.75 \times 10^{-4}$	$6.04 \times 10^{-4}$	$5.43 \times 10^{-4}$	-	0.03
		2.74	$2.66 \times 10^{-4}$	$1.68 \times 10^{-4}$	$1.86 \times 10^{-4}$	-	0.1
		5.48	$6.01 \times 10^{-5}$	$4.07 \times 10^{-5}$	$6.56 \times 10^{-5}$	-	1
		$p$	$<10^{-4}$	0.002	0.001	-	

**Table VII. Simulation results and two-way statistical analyses of the simulation data in terms of  $p$  values of normalized conductivity of composite  $\text{Li}(\text{Ni}_{0.8}\text{Co}_{0.15}\text{Al}_{0.05})\text{O}_2$  with 40% porosity and 50% porosity.**

Porosity	$\text{Li}(\text{Ni}_{0.8}\text{Co}_{0.15}\text{Al}_{0.05})\text{O}_2$	PVDF/C	Graphite (%)				$p$
			0	2.5	5	7.5	
40%	30%	1.21	$4.03 \times 10^{-3}$	$5.48 \times 10^{-3}$	$7.81 \times 10^{-3}$	$1.21 \times 10^{-2}$	0.001
		2.74	$1.09 \times 10^{-3}$	$1.54 \times 10^{-3}$	$2.32 \times 10^{-3}$	$4.34 \times 10^{-3}$	0.002
		5.48	$2.33 \times 10^{-4}$	$3.33 \times 10^{-4}$	$5.28 \times 10^{-4}$	$1.22 \times 10^{-4}$	0.005
		$p$	$<10^{-4}$	$<10^{-4}$	$<10^{-4}$	$<10^{-4}$	
	40%	1.21	$2.09 \times 10^{-3}$	$3.26 \times 10^{-3}$	$3.87 \times 10^{-3}$	$3.75 \times 10^{-3}$	0.1
		2.74	$5.64 \times 10^{-4}$	$8.94 \times 10^{-4}$	$1.10 \times 10^{-3}$	$1.14 \times 10^{-3}$	0.2
		5.48	$1.21 \times 10^{-4}$	$1.93 \times 10^{-4}$	$2.42 \times 10^{-4}$	$2.69 \times 10^{-4}$	0.4
		$p$	$<10^{-4}$	$<10^{-4}$	0.1	0.003	
	50%	1.21	$1.24 \times 10^{-3}$	$9.47 \times 10^{-4}$	$1.18 \times 10^{-4}$	-	$<10^{-4}$
		2.74	$3.34 \times 10^{-4}$	$2.63 \times 10^{-4}$	$4.11 \times 10^{-5}$	-	$<10^{-4}$
		5.48	$7.18 \times 10^{-5}$	$5.80 \times 10^{-5}$	$1.51 \times 10^{-5}$	-	$<10^{-4}$
		$p$	$<10^{-4}$	$<10^{-4}$	0.2	-	
50%	30%	1.21	$1.92 \times 10^{-3}$	$3.30 \times 10^{-3}$	$2.62 \times 10^{-3}$	$6.34 \times 10^{-3}$	0.005
		2.74	$5.19 \times 10^{-4}$	$9.65 \times 10^{-4}$	$7.39 \times 10^{-4}$	$2.26 \times 10^{-3}$	0.009
		5.48	$1.11 \times 10^{-4}$	$2.17 \times 10^{-4}$	$1.61 \times 10^{-4}$	$5.85 \times 10^{-4}$	0.02
		$p$	$<10^{-4}$	$<10^{-4}$	$<10^{-4}$	0.001	
	40%	1.21	$1.13 \times 10^{-3}$	$9.93 \times 10^{-4}$	$1.67 \times 10^{-4}$	-	$<10^{-4}$
		2.74	$3.06 \times 10^{-4}$	$2.71 \times 10^{-4}$	$5.08 \times 10^{-5}$	-	$<10^{-4}$
		5.48	$6.56 \times 10^{-5}$	$5.87 \times 10^{-5}$	$1.49 \times 10^{-5}$	-	0.001
		$p$	0.001	$<10^{-4}$	$<10^{-4}$	-	

conductivity of the surface and therefore fail to create a percolated network of spheres. Improvements from addition of larger particle conductive additives is only obvious in cases with 40% porosity and 30% active material for the four active material systems and cases with 50% porosity and 30% active material for  $\text{Li}(\text{Ni}_{0.8}\text{Co}_{0.15}\text{Al}_{0.05})\text{O}_2$  and  $\text{Li}(\text{Ni}_{1/3}\text{Co}_{1/3}\text{Mn}_{1/3})\text{O}_2$  systems.

In Table IX we compared the effective conductivity of two different loading schemes around active-material particle. In both load-

ing schemes, the PVDF/carbon black composite coating was included. From this table, we see that addition of a carbon nanofilm coating around active-material particles does not significantly improve laminate conductivity. Moreover, binder is required to maintain structural integrity of the composite electrode, regardless of other additives or treatments. Because of the relatively low conductivity of the binder, carbon black addition seems a reasonable way of improving conduction.

**Table VIII. Simulation results and two-way statistical analyses of the simulation data in terms of  $p$  values of normalized conductivity of composite  $\text{Li}(\text{Ni}_{1/3}\text{Co}_{1/3}\text{Mn}_{1/3})\text{O}_2$  with 40% porosity and 50% porosity.**

Porosity	$\text{Li}(\text{Ni}_{1/3}\text{Co}_{1/3}\text{Mn}_{1/3})\text{O}_2$	PVDF/C	Graphite (%)				$p$
			0	2.5	5	7.5	
40%	30%	1.21	$3.94 \times 10^{-3}$	$5.62 \times 10^{-3}$	$6.31 \times 10^{-3}$	$8.99 \times 10^{-3}$	0.006
		2.74	$1.06 \times 10^{-3}$	$1.59 \times 10^{-3}$	$1.87 \times 10^{-3}$	$3.09 \times 10^{-3}$	0.003
		5.48	$2.27 \times 10^{-4}$	$3.46 \times 10^{-4}$	$4.24 \times 10^{-4}$	$8.23 \times 10^{-4}$	0.004
		$p$	0.001	$<10^{-4}$	$<10^{-4}$	$<10^{-4}$	
	40%	1.21	$3.06 \times 10^{-3}$	$3.51 \times 10^{-3}$	$5.16 \times 10^{-3}$	$4.24 \times 10^{-3}$	0.001
		2.74	$8.26 \times 10^{-4}$	$9.70 \times 10^{-4}$	$1.55 \times 10^{-3}$	$1.30 \times 10^{-3}$	0.001
		5.48	$1.76 \times 10^{-4}$	$2.09 \times 10^{-4}$	$3.53 \times 10^{-4}$	$2.92 \times 10^{-4}$	0.001
		$p$	$<10^{-4}$	$<10^{-4}$	$<10^{-4}$	$<10^{-4}$	
	50%	1.21	$1.25 \times 10^{-3}$	$8.41 \times 10^{-4}$	$3.04 \times 10^{-7}$	-	0.8
		2.74	$3.37 \times 10^{-4}$	$2.29 \times 10^{-4}$	$2.94 \times 10^{-7}$	-	0.5
		5.48	$7.20 \times 10^{-5}$	$4.91 \times 10^{-5}$	$2.60 \times 10^{-7}$	-	0.4
		$p$	$<10^{-4}$	$<10^{-4}$	1	-	
50%	30%	1.21	$2.83 \times 10^{-3}$	$3.97 \times 10^{-3}$	$3.97 \times 10^{-3}$	$4.95 \times 10^{-3}$	0.01
		2.74	$6.43 \times 10^{-4}$	$1.12 \times 10^{-3}$	$1.13 \times 10^{-3}$	$1.60 \times 10^{-3}$	0.01
		5.48	$1.37 \times 10^{-4}$	$2.43 \times 10^{-4}$	$2.49 \times 10^{-4}$	$3.77 \times 10^{-4}$	0.01
		$p$	0.008	$<10^{-4}$	0.001	$<10^{-4}$	
	40%	1.21	$5.86 \times 10^{-4}$	$1.03 \times 10^{-3}$	$6.98 \times 10^{-5}$	-	0.002
		2.74	$1.58 \times 10^{-4}$	$2.86 \times 10^{-4}$	$1.92 \times 10^{-5}$	-	0.002
		5.48	$3.38 \times 10^{-5}$	$6.17 \times 10^{-5}$	$4.22 \times 10^{-5}$	-	0.002
		$p$	0.004	$<10^{-4}$	$<10^{-4}$	-	

**Table IX. Comparison between LiFePO<sub>4</sub> with and without nanofilm coating; cathode system with 30% active material, 40% porosity, 7.5% graphite, 10.15% carbon black, and 12.35% PVDF.**

Active material	LiFePO <sub>4</sub> with nanofilm coating	LiFePO <sub>4</sub> without nanofilm coating
Bulk conductivity (S/m)	$5.91 \times 10^{-1}$	$10^{-9}$
Normalized effective conductivity	$1.47 \times 10^{-2}$	$1.16 \times 10^{-2}$

### Conclusion

A method is presented to simulate the particulate system of conductive additives in Li-ion battery cathodes and investigate the relationships among types of additives in improving conduction. The error due to size effect of the domain was negligible for the selected ratio  $L/d > 2.5$ . Variances in simulation results mainly arose from differences in arrangements of random structures. The model is capable of generating realistic microstructures of the cathode system and robustly predicting the effective conductivity with different types of conductive additives, e.g., conductive surface coatings and larger dispersed conductive additives.

A key finding was that the conductive coatings have a strong influence on overall conductivity because they substantially reduce contact resistance. Percolation was achieved due to the volume fraction of active material ( $\geq 30\%$ ), which is greater than the theoretical percolation threshold (29%) for 3D spherical particulate systems. Generally, using carbon black/PVDF composite coatings is more advantageous than addition of conductors (e.g., graphite) to composite cathodes for all baseline materials. Overall, the best conductivity in each system studied was achieved by combination of 30% active material, 40% porosity, 7.5% graphite, 10.15% carbon black, and 12.35% PVDF.

Neither surface nor bulk modifications of active-material particle conductivities seem desirable targets for improvement of laminate conductivity for the ranges of materials studied. Our simulation results showed that the difference among the highest normalized conductivities of each system is only within 1 order in magnitude, while the conductivities of four active materials range from  $5.91 \times 10^{-1}$  to  $5.56 \times 10^{-4}$  S/m. Even with only 10% coatings (4.51% carbon black, 5.49% PVDF) in studied cases of 50% porosity and 40% active material, the overall conductivity was increased by at least 14.9 S/m, a value 25 times larger than the bulk conductivity of the active material. Further, an improvement of approximately 3 orders of magnitude in conductivity (PVDF/C:  $7.6 \times 10^2$  S/m vs LiFePO<sub>4</sub>:  $5.91 \times 10^{-1}$  S/m) of the active material would be required to offer substantial improvement in overall conductivity.

As part of future work, the trade-off between conductivity and capacity will be considered. Our next step is to incorporate the effect of improved conductivity in the simulations of battery performance in order to further optimize cathode design.

### Acknowledgments

This work was generously supported by the Department of Energy BATT Program (Dr. Tien Duong, Program Director, DOE). Additional support was provided by the Ford Motor Company (Ted Miller and Kent Snyder, Program Directors), and the Army Research Office (Dr. Bruce LaMattina, Program Director). We gratefully acknowledge these sponsors and colleagues.

University of Michigan assisted in meeting the publication costs of this article.

### References

1. K. Ozawa, *Solid State Ionics*, **69**, 212 (1994).
2. C. Delmas and I. Saadoune, *Solid State Ionics*, **53-56**, 370 (1992).
3. C. Delmas, I. Saadoune, and A. Rougier, *J. Power Sources*, **44**, 595 (1993).
4. A. Rougier, I. Saadoune, P. Gravereau, P. Willmann, and C. Delmas, *Solid State Ionics*, **90**, 83 (1996).
5. J. R. Dahn, W. W. Fuller, M. Obrovac, and U. von Sacken, *Solid State Ionics*, **69**, 265 (1994).
6. Z. Zhang, D. Fouchard, and J. R. Rea, *J. Power Sources*, **70**, 16 (1998).
7. Z. Liu, J. Y. Lee, and H. J. Linder, *J. Power Sources*, **97-98**, 361 (2001).
8. R. Dominko, M. Gaberscek, J. Drofenik, M. Bele, and S. Pejovnik, *Electrochem. Solid-State Lett.*, **4**, 187 (2001).
9. S. Mandal, J. M. Amarilla, J. Ibanez, and J. M. Rojo, *J. Electrochem. Soc.*, **148**, A24 (2001).
10. A. Momchilov, A. Trifonova, B. Banov, B. Pourecheva, and A. Kozawa, *J. Power Sources*, **81-82**, 566 (1999).
11. A. S. Skapin, M. Gaberscek, R. Dominko, M. Bele, J. Drofenik, and J. Jamnik, *Solid State Ionics*, **167**, 229 (2004).
12. M. G. Lazarraga, S. Mandal, J. Ibanez, J. M. Amarila, and J. M. Rojo, *J. Power Sources*, **115**, 315 (2003).
13. S. L. Bewlay, K. Konstantinov, G. X. Wang, S. X. Dou, and H. K. Liu, *Mater. Lett.*, **58**, 1788 (2004).
14. K. Zaghbi, J. Shim, A. Guerfi, P. Charest, and K. A. Striebel, *Electrochem. Solid-State Lett.*, **8**, A207 (2005).
15. C. M. Julien, K. Zaghbi, A. Mauger, M. Massot, A. Massot, A. Ait-Salah, M. Selmane, and F. Gendron, *J. Appl. Phys.*, **100**, 063511 (2006).
16. C.-W. Wang, A. M. Sastry, K. A. Striebel, and K. Zaghbi, *J. Electrochem. Soc.*, **152**, A1001 (2005).
17. R. J. Gummow, A. de Kock, and M. M. Thackeray, *Solid State Ionics*, **69**, 59 (1994).
18. J. P. Tu, H. M. Wu, X. T. Chen, Y. Li, X. B. Zhao, and G. S. Cao, *J. Electroanal. Chem.*, **586**, 180 (2006).
19. A. K. Padhi, K. S. Nanjundaswamy, C. Masquelier, and J. B. Goodenough, *J. Electrochem. Soc.*, **144**, 2581 (1997).
20. C. H. Mi, X. G. Zhang, X. B. Zhao, and H. L. Li, *J. Alloys Compd.*, **424**, 327 (2006).
21. S.-W. Song, G. V. Zhuang, and P. N. Ross, Jr., *J. Electrochem. Soc.*, **151**, A1162 (2004).
22. I. Belharouak, D. Vissers, and K. Amine, *J. Electrochem. Soc.*, **153**, A2030 (2006).
23. Z. Lu and J. R. Dahn, *J. Electrochem. Soc.*, **148**, 237 (2001).
24. P. He, H. Wang, L. Qi, and T. Osaka, *J. Power Sources*, **160**, 627 (2006).
25. K. Zaghbi, P. Charest, A. Guerfi, J. Shim, M. Perrier, and K. Striebel, *J. Power Sources*, **134**, 124 (2004).
26. J. Quintanilla and S. Torquato, *Phys. Rev. E*, **54**, 5331 (1996).
27. J. Quintanilla and S. Torquato, *Adv. Appl. Probab.*, **29**, 327 (1997).
28. Y.-B. Yi and A. M. Sastry, *Phys. Rev. E*, **66**, 066130 (2002).
29. Y.-B. Yi and A. M. Sastry, *Proc. R. Soc. London, Ser. A*, **460**, 2353 (2004).
30. C.-W. Wang, K. A. Cook, and A. M. Sastry, *J. Electrochem. Soc.*, **150**, A385 (2003).
31. C.-W. Wang, A. M. Sastry, K. A. Striebel, and K. Zaghbi, *J. Electrochem. Soc.*, **152**, A1001 (2005).
32. Y.-B. Yi, C.-W. Wang, and A. M. Sastry, *J. Eng. Mater. Technol.*, **128**, 73 (2006).
33. J. Moskon, R. Dominko, M. Gaberscek, R. Cerc-Korosec, and J. Jamnik, *J. Electrochem. Soc.*, **153**, A1805 (2006).
34. Matweb, <http://www.matweb.com> (05/31/2006).
35. J. Guan and M. Liu, *Solid State Ionics*, **110**, 21 (1998).
36. S.-Y. Chung, J. T. Bloking, and Y.-M. Chiang, *Nat. Mater.*, **1**, 123 (2002).
37. P. Meakin and R. Jullien, *J. Phys. (France)*, **48**, 1651 (1987).
38. L. Liu and Y. Yuan, *J. Mater. Sci. Lett.*, **19**, 841 (2000).
39. G. Fu and W. Dekelbab, *Powder Technol.*, **133**, 147 (2003).
40. E. Santiso and E. A. Muller, *Mol. Phys.*, **100**, 2461 (2002).
41. V. Falk and U. D'Ortona, *Powder Technol.*, **128**, 229 (2002).
42. N. V. Kosova, N. F. Uvarov, E. T. Devyatkina, and E. G. Avvakumov, *Solid State Ionics*, **135**, 107 (2000).
43. J. Molenda, K. Swierczek, M. Molenda, and J. Marzec, *Solid State Ionics*, **135**, 53 (2000).
44. P. B. Joshi and P. Ramakrishnan, *Materials for Electrical and Electronic Contacts*, p. 90-91, Science Publishers, Enfield (2004).
45. F. M. Smits, *Bell Syst. Tech. J.*, **37**, 711 (1958).
46. D. A. G. Bruggeman, *Ann. Phys.*, **24**, 636 (1935).
47. D. Guy, B. Lestriez, R. Bouchet, and D. Guyomard, *J. Electrochem. Soc.*, **153**, A679 (2006).
48. ABAQUS/STANDARD v.6.6, ABAQUS, Inc., Providence, RI.
49. SPSS v.13, SPSS Inc., Chicago, IL.
50. A. A. Gusev, *J. Mech. Phys. Solids*, **45**, 1449 (1997).